RSC Advances

ROYAL SOCIETY OF CHEMISTRY

www.rsc.org/advances

Y-doped $PbWO_4$ mesocrystals with controllable morphologies, from convex quadrangle to concave erythrocyte, are obtained by simply increasing Y^{3+} doping concentrations.

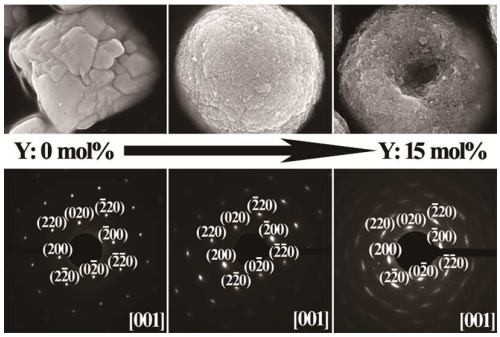

RSC Advances

RSCPublishing

COMMUNICATION

Doping-Induced Evolutions of $PbWO_4$ Mesocrystals and Its Optical Properties

Cite this: DOI: 10.1039/xoxxoooooox

Ying Xiong,[*,a,b] Bing Wang,[a] Hao Zhuang,[b] Xin Jiang,[b] Guohua Ma,[c] Yong Yi,[a] Wenyuan Hu,[a] and Yuanlin Zhou[a]

Received ooth January 2012,
Accepted ooth January 2012

DOI: 10.1039/xoxxoooooox

www.rsc.org/

Y-doped $PbWO_4$ mesocrystals with controllable morphologies, from convex quadrangle to concave erythrocyte, which exhibit tunable optical properties, are obtained by simply increasing Y^{3+} doping concentrations. A doping-induced structural disorder mechanism was tentatively proposed to understand the evolutions of $PbWO_4$ mesocrystals.

Mesocrystals, a novel hierarchical structure, are composed of individual nanoparticles building blocks *via* a non-classical particle-mediated crystallization pathway.[1] The appearance of the mesocrystals opens up the possibilities in designing and fabricating new materials and devices.[2] In the synthesis of most well-known mesocrsytals, organic additives such as surfactants, polyelectrolytes and biomacromolecules have been employed as stabilizers or inducers.[3] But it is an arduous work to elucidate the exact effects of these additives on the formation of mesocrystals. Moreover, the incorporation of these additives would not beneficial to the optical or electric properties of mesocrystals.[4] In this regard, to synthesize mesocrystals without the addition of organic matrices can provide new insights in understanding their formation mechanism and modifying their properties.

In recent years, intensive researches have revealed that impurity doping can not only tune electronic, magnetic and optical properties of *colloidal nanocrystals*, but also have significant impact on its nucleation and growth process.[5-6] The latter provided a convenient route to modify the phase structures, sizes and shapes. Doping-induced modification of surface charge density[5] and generation of transient electric dipoles[6] were successively proposed to shed some light on the possible mechanism. Nevertheless, all of above mentioned reports mainly focused on the issues how impurity doping modified *colloidal nanocrystals*' nucleation and growth process. Until now, the investigations on the effect of impurity doping on the *mesocrystals* formation, especially the mutual orientation between primary nanocrystals, is still lacking.

$PbWO_4$, an important member of tungstate family, exhibits high potential in various applications such as scintillator in high-energy physics, laser and stimulated-Raman-scattering active media.[7] Several researches have recently shown that $PbWO_4$ synthesized through wet chemical method tends to form a highly ordered hierarchical or mesoscale structures.[8] But it strongly relied on the kind of surfactants used and the formation mechanism about these structures were not completely clear and even contradictory. So far it is still a challenge to develop a facile approach without using surfactants to synthesize $PbWO_4$ mesocrystals with controllable morphology. In this communication, we show that in the synthesis of $PbWO_4$ mesocrystals, introduction of Y^{3+} dopants leads to dramatic morphological evolution. Depending on the relative concentrations of dopants, Y-doped $PbWO_4$ mesocrystals with well-defined shapes, from convex quadrangle and concave erythrocyte, were obtained through a simple and facile co-precipitation method. A doping-induced structural disorder hypothesis was proposed to understand the evolutions of $PbWO_4$ mesocrystals.

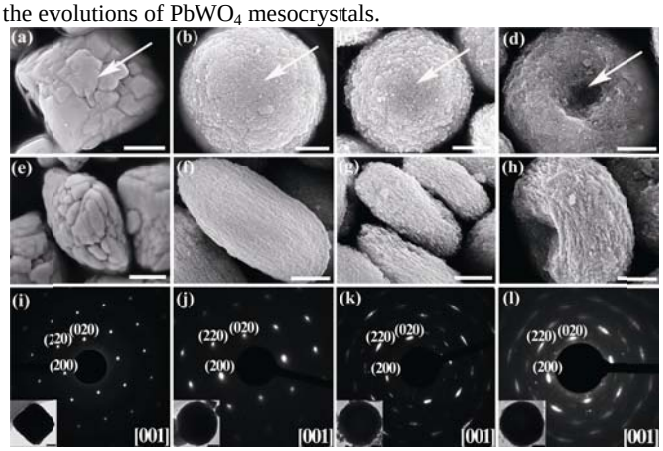

Fig. 1 Top- and side-view FESEM images and SAED patterns of a single Y-doped $PbWO_4$ mesocrystals. (a,e,i) 0 mol%; (b,f,j) 5 mol%; (c,g,k) 10 mol%; (d,h,l) 15 mol%. The scale bar in all images corresponds to 400 nm. All of SAED patterns were taken from an individual product shown in the inset.

Low-magnification FESEM images (Fig. S1, ESI†) reveal all of $PbWO_4$ samples have a uniform shape. So high-magnification FESEM images in Fig. 1, recorded from a single product, represent the entire sample population. Without deliberately added Y^{3+} ions, the FESEM images (Fig. 1a,e) shows the products have convex and quadrangle shape, which are composed of densely packed nanocrystals and clear boundaries between nanocrystals can be seen. SAED pattern (Fig. 1i) consists of individual diffraction spots along the [001] axis-zone, suggesting a single-crystalline nature. This is

further verified by fast Fourier transfer (FFT) diffractogram (the inset of Fig. 2a). Based on the aggregation-like morphology and single-crystalline diffraction, we therefore concluded the convex quadrangles to be mesocrystals, in which primary $PbWO_4$ nanocrystals was spontaneously aligned and oriented along the same crystallographic direction.[1,3] The fact that the nanocrystals in the vicinity of boundaries have the parallel lattice fringes with a spacing of 0.19 nm (Fig. 2a and 2b) also demonstrates the orientation feature in $PbWO_4$ mesocrystals.

XRD patterns of Y-doped $PbWO_4$ mesocrystals with different Y^{3+} concentrations reveal that all of products have pure tetragonal scheelite structure and the increase of Y^{3+} concentrations results in decreasing in crystallinity and grain size of primary $PbWO_4$ nanocrystals (Fig. S2 and Table S1, ESI†). With increasing Y^{3+} dopant concentrations, the shape of as-obtained $PbWO_4$ mesocrystals gradually transforms to round and concave, marked by white arrows in Fig. 2. In the presence of Y^{3+} dopant ions (15 mol%), novel erythrocyte-like shape can be obtained in $PbWO_4$ samples (Fig. 2d and 2h). Moreover, higher Y^{3+} doping concentration results in smaller nanocrystals in $PbWO_4$ samples, well consistent with the XRD results (Table S1, ESI†), and induces more distinct layered arrangement between these nanocrystals.

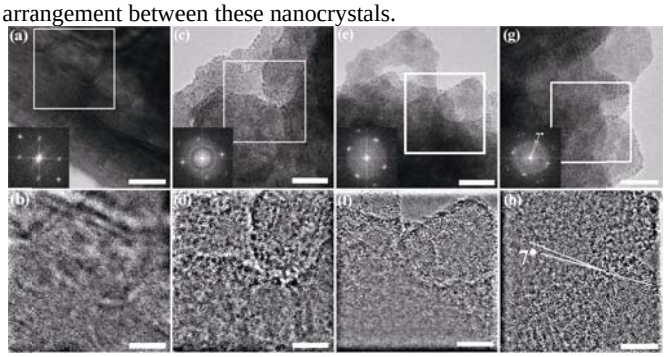

Fig. 2 HRTEM images and corresponding FFT diffractograms (the inset) as well as IFFT images of Y-doped $PbWO_4$ mesocrystals. (a,b) 0 mol%; (c,d) 5 mol%; (e,f) 10 mol%; (g,h) 15 mol%. FFT and IFFT obtained from the white-square area of HRTE image.

For $PbWO_4$ mesocrystals with 5 mol% Y^{3+} ions, SAED pattern still reveals a single crystalline nature (Fig. 1j), but the individual diffraction spots feature a slight deformation, indicating there may be slightly a small angle mismatch between adjacent primary nanocrystals. As shown in Fig. 2c and 2d, boundaries between adjacent nanocrystals become clearer due to the decrease in the grain size of primary $PbWO_4$ nanocrsytals and the nanocrytals in the vicinity of boundaries also have parallel lattice fringes with a spacing of 0.27 nm. Further increasing in Y^{3+} doping concentrations, this orientation mismatch becomes more obvious (Fig. 1k and 1l), in which discontinuous diffraction rings can also be seen besides the bright, arc-shaped individual diffraction spots. This change in the orientation mismatch can also be found in the corresponding FFT diffratogram (Fig. 2e and 2g). More obviously, from the IFFT image in Fig. 2h, orientation mismatch about 7° between two adjacent nanocrystals can be directly observed. So, during the formation of $PbWO_4$ mesocrsytals, Y^{3+} doping could obviously modify the mutual orientation process of primary nanocrystals.

The existence of a net magnetic or electric dipole, which, in the latter case, can often develop as a result of adsorption of additives onto specific faces of the primary nanocrystals, can act as a driving force for the mesocrystals formation.[3] In the absence of any organic additives, $PbWO_4$ mesocrystals could be formed, as shown in Fig. 1. So there was reason to believe that the formation of $PbWO_4$ mesocrystals could possibly originate from the existence of intrinsic driving forces in $PbWO_4$ such as net electric dipoles. As shown in Fig. 3, the W^{6+} ion in the $[WO_4]$ tetrahedron and the Pb^{2+} ion in the $[PbO_8]$ pseudocube are always located at a same layer, from the point of crystallographic axis directions, and the adjacent layers containing metal ions are isolated by pure oxygen ions layers. This anisotropic ionic stacking feature further results in some specific planes consisted of either pure metal ions such as (004), (200) and (220) or pure oxygen ions such as (400).

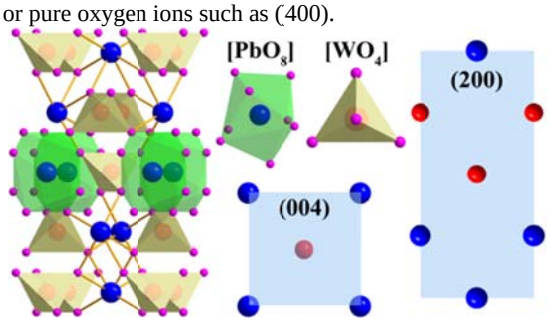

Fig. 3 (*left*) 1 × 1 × 1 unit cell of tetragonal $PbWO_4$ structure; (*middle upper*) $[PbO_8]$ and $[WO_4]$ polyhedrons; (*middle bottom* and *right*) 2D atomic configurations in the (004) and (200) planes. The blue, red and pink spheres represent lead, tungsten and oxygen atoms, respectively.

Due to the differences in ionic radius and valence, the substitution of Pb^{2+} by Y^{3+} ions could result in the deformation of $[PbO_8]$ polyhedra and the existence of positively charged defects Y_{Pb}^{+}, which further induced the distortion of adjacent $[WO_4]$ tetrahedra and the appearance of negatively charge defects. These changes would become more obvious at higher Y^{3+} doping concentrations. These deformation and/or distortion as well as charged point defects could possibly induce the charge distributions' variation of these pure metal or oxygen crystallographic planes in primary $PbWO_4$ nanoparticles, and substantially modify the driving force (net electric dipoles) for their directional or oriented aggregation. Based on this speculation, it may seem reasonable that increasing in Y^{3+} doping concentrations resulted in the increase of orientation mismatch between primary $PbWO_4$ nanoparticles and the continuous morphological evolutions of $PbWO_4$ mesocrystals. More importantly, the similar doping-induced continuous morphological evolution in $PbWO_4$ mesocrystals could be also seen in other trivalent rare-earth doping ions such as La^{3+}, Nd^{3+}, and Gd^{3+}, even in divalent alkaline-earth doping ions such as Sr^{2+}, as shown in Figure S3, ESI†. Nevertheless, owing to the differences in ionic radius, polarizability and valence of these dopant ions, there are some discrepancies in specific morphologies of as-obtained doped $PbWO_4$ mesocrystals,[6a] and theoretical simulations about how impurity doping modify the charge distribution of special crystallographic planes and the further mesocrystals formation will be the focus of our following work.

According to previous reports, optical properties are very sensitive to local lattice symmetry and can be used as an intrinsic probe to map the structural variations in scheelite crystals.[9-11] In the case of undoped $PbWO_4$ mesocrystals (Fig. 4a), six Raman bands corresponding to the internal modes inside the $[WO_4]$ molecular groups can be seen.[9b,10] However, with adding Y^{3+} doping ions, the Raman intensity decreases rapidly, indicating the increase in the imperfection of $[WO_4]$ molecular groups.[9c,10c] Moreover, two vibration bands at 354.6 and 764.4 cm^{-1}, corresponding to non-symmetrical bonding $\nu_4(B_g)$ and stretching $\nu_3(B_g)$, gradually decrease in intensities and are finally merged with the bonding $\nu_4(E_g)$ and $\nu_3(E_g)$ to form a broadband peak (the inset of Figure 3a). It is likely that the merging of the E_g and B_g components is connected with the increase of the distortion of $[WO_4]$ molecular groups with increasing Y^{3+} doping concentrations.[10c] As a result, the change in Raman spectra strongly confirmed the above-mentioned doping-induced structural disorder speculation.

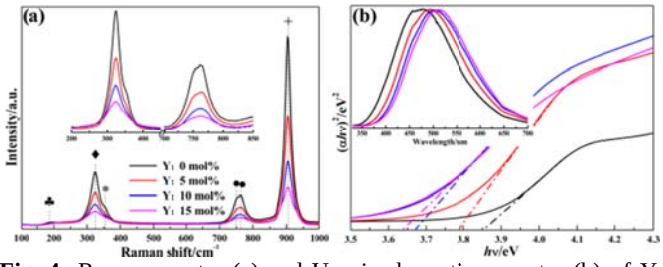

Fig. 4 Raman spectra (a) and Uv-vis absorption spectra (b) of Y-doped $PbWO_4$ mesocrystals with different Y^{3+} doping concentrations. The inset of (b) is the normalized PL spectra.

In the UV-vis spectra (Figure 4b), the optical gap energy (E_g) value of undoped $PbWO_4$ mesocrystals is about 3.85 eV. With increasing Y^{3+} concentrations, the E_g shifts gradually toward lower values, and in the case of 15 mol% Y^{3+} ions, it is only 3.63 eV. In theory, the decrease in the E_g value is associated with the existence of intermediary energy levels within the band gap due to impurity atoms and/or structural defects of host lattices. For the scheelite lead tungstate, a great number of theoretical calculations revealed that the band gap strongly relied on the O $2p\pi$ states and W $5d$ states,[11] and a little displacement of W atoms and/or distortion of W-O bonds in $[WO_4]$ molecular groups could induce a marked change of band gap.[10a,11] As a result, the continuous decrease in the E_g value as a function of Y^{3+} doping concentrations could be mainly attributed to the variation of state density distribution of O $2p\pi$ and W $5d$ states in $[WO_4]$ molecular groups, originating from the doping-dependent distortion of $[WO_4]$ tetrahedron.

The doping-induced changes in energy level of band gap were also reflected on photoluminescence (PL) properties. As shown in the inset of Figure 4b, all of $PbWO_4$ mesocrystals emit broad bands in the visible spectrum region and the maximum value of the broadband emission progressively shifts from 479 nm to 513 nm, with increasing Y^{3+} doping concentrations. These broadband emissions are typical of a multiphonon or multilevel process and can be well fitted into three Gaussian components (Figure S4, ESI†), corresponding to the blue, green and yellow emissions, respectively. Interestingly, each Gaussian emission peak shifts toward high wavelength direction with increasing Y^{3+} concentration. This red-shift of blue, green and yellow emission as a function of Y^{3+} concentrations could be also considered as a concrete manifestation of doping-induced structure disorder.

In conclusion, we demonstrated the morphology and microstructure of $PbWO_4$ mesocrystals could be effectively modified by impurity doping of Y^{3+} ions. Based on the intrinsic anisotropic ionic stacking feature, a doping-induced structural disorder hypothesis was proposed to understand the underlying mechanism. A deeper understanding of the doping-induced mesocrystal evolutions may help us towards designing new synthesis strategies for other inorganic materials in future and extending the views about mesocrystal formation in a much broader.

This work was supported by the National Natural Science Foundation of China (Grant No. 11205127), NSAF (Grant No. U1330127 and 11176026), Youth Innovation Research Team of Sichuan for Carbon Nanomaterials (Grant No. 2011JTD0017), Open Foundation of State Key Laboratory Cultivation Base for Nonmetal Composites and Functional Materials (Grant No. 11zxfk26) and a scholarship under the State Scholarship Fund by the China Scholarship Council (2011851658).

Notes and references

[a] State Key Laboratory Cultivation Base for Nonmetal Composites and Functional Materials, Southwest University of Science & Technology, Mianyang 621010, P. R. China
[b] Institute of Materials Engineering, University of Siegen, Paul-Bonatz-Str. 9-11, 57076 Siegen, Germany
[c] Analytical and Testing Center, Southwest University of Science & Technology, Mianyang 621010, P. R. China
† Electronic Supplementary Information (ESI) available: Experimental details and Fig. S1-S4. See DOI: 10.1039/c000000x/

1 R. Q. Song, H. Cölfen, *Adv. Mater.* 2010, **22**, 1301-1330.
2 (*a*) X. L. Wu, S. J. Xiong, Z. Liu, J. Chen, J. C. Shen, T. H. Li, P. H. Wu, P. K. Chu, *Nature Nanotech.* 2011, **6**, 103-106; (*b*) S. Z. Deng, V. Tjoa, H. M. Fan, H. R. Tan, D. C. Sayle, M. Olivo, S. Mhaisalkar, J. Wei, C. H. Sow, *J. Am. Chem. Soc.* 2012, **134**, 4905-4917.
3 (*a*) M. H. Liu, Y. H. Tseng, H. F. Greer, W. Zhou, C. Y. Mou, *Chem. Eur. J.* 2012, **18**, 16104-16113; (*b*) Z. Liu, X. D. Wen, X. L. Wu, Y. J. Gao, H. T. Chen, J. Zhu, P. K. Chu, *J. Am. Chem. Soc.* 2009, **131**, 9405-9412.
4 Y. Jin, J. H. Zhang, S. Z. Lu, H. F. Zhao, X. Zhang, X. J. Wang, *J. Phys. Chem. C* 2008, **112**, 5860-5964.
5 (*a*) D. J. Norris, A. L. Efros and S. C. Erwin, *Science*, 2008, **319**, 1776-1779; (*b*) D. Q. Chen and Y. S. Wang, *Nanoscale*, 2013, **5**, 4621-4637; (*c*) X. D. Feng, D. C. Sayle, Z. L. Wang, M. S. Paras, B. Santora, A. C. Sutorik, T. X. Sayle, Y. Yang, Y. Ding, X. D. Wang and Y. S. He, *Science*, 2006, **312**, 1504-1508; (*d*) Y. Ding, J. Gu, J. Ke, Y. W. Zhang and C. H. Yan, *Angew. Chem. Int. Ed.*, 2011, **50**, 12330-12334; (*e*) Y. F. Yang, Y. Z. Jin, H. P. He, Q. L. Wang, Y. Tu, H. M. Lu and Z. Z. Ye, *J. Am. Chem. Soc.*, 2010, **132**, 13381-13394.
6 (*a*) F. Wang, Y. Han, C. S. Lim, Y. H. Lu, J. Wang, J. Xu, H. Y. Chen, C. Zhang, M. H. Hong and X. G. Liu, *Nature*, 2010, **463**, 1061-1065; (*b*) D. Q. Chen, Y. L. Yu, F. Huang, P. Huang, A. P. Yang and Y. S. Wang, *J. Am. Chem. Soc.*, 2010, **132**, 9976-9978; (*c*) H. L. Qiu, G. Y. Chen, R. W. Fan, C. Cheng, S. W. Hao, D. Y. Chen and C. H. Yang, *Chem. Commun.*, 2011, **47**, 9648-9650; (*d*) D. Q. Chen, P. Huang, Y. L. Yu, F. Huang, A. P. Yang and Y. S. Wang, *Chem. Commun.*, 2011, **47**, 5801-5803.
7 H. Tang, C. S. Li, H. J. Song, X. F. Yang and X. H. Yan, *CrystEngComm* 2011, **13**, 5119-5124.
8 (*a*) Q. Zhang, W. T. Yao, X. Y. Chen, L. W. Zhu, Y. B. Fu, G. B. Zhang, L. S. Sheng and S. H. Yu, *Cryst. Growth & Design*, 2007, **7**, 1423-1431; (*b*) F. Dong, Y. Huang, S. C. Zou, J. Liu and S. C. Lee, *J. Phys. Chem. C*, 2011, **115**, 241-247; (*c*) C. L. Yu, F. F. Cao, X. Li, G. Li, Y. Xie, J. C. Yu, Q. Shu, Q. Z. Fan and J. C. Chen, *Chem. Eng. J.*, 2013, **219**, 86-95; (*d*) B. Liu, S. H. Yu, L. J. Li, Q. Zhang, F. Zhang and K. Jiang, *Angew. Chem. Int. Ed.*, 2004, **43**, 4745-4750; (*e*) X. H. Guo, J. P. Yang, Y. H. Deng, H. Wei and D. Y. Zhao, *Eur. J. Inorg. Chem.*, 2010, **11**, 1736-1742.
9 (*a*) T. T. Basiev, A. A. Sobol, Yu. K. Voronko and P. G. Zverev, *Opt. Mater.*, 2000, **15**, 205-216; (*b*) L. S. Cavalcante, J. C. Sczancoski, V. C. Albarici, J. M. E. Matos, J. A. Varela and E. Longo, *Mater. Sci. Engin. B*, 2008, **150**, 18-25; (*c*) M. Anicete-Santos, F. C. Picon, C. N. Alves, P. S. Pizani, J. A. Varela and E. Longo, *J. Phys. Chem. C*, 2011, **115**, 12180-12186.
10 (*a*) L. S. Cavalcante, F. M. C. Batista, M. A. P. Almeida, A. C. Rabelo, L. C. Nogueira, N. C. Batista, J. A. Varela, M. R. M. C. Santos, E. Longo and M. Siu Li, *RSC Adv.*, 2012, **2**, 6438-6454; (*b*) J. Geng, J. J. Zhu, D. J. Lu and H. Y. Chen, *Inorg. Chem.*, 2006, **45**, 8403-8407; (*c*) L. S. Cavalcante, J. C. Sczancoski, L. F. Lima, Jr., J. W. M. Espinosa, P. S. Pizani, J. A. Varela and E. Longo, *Crys. Growth & Design*, 2009, **9**, 1002-1012.
11 (*a*) M. Anicete-Santos, E. Orhan, M. A. M. A. de Maurera, L. G. P. Simões, A. G. Souza, P. S. Pizani, E. R. Leite, J. A. Varela, J. Andrés, A. Beltrán and E. Longo, *Phys. Rev. B*, 2007, **75**, 165105; (*b*) Y. Zhang, N. A. W. Holzwarth and R. T. Williams, *Phys. Rev. B*, 1998, **57**, 12738-12750; (*c*) L. S. Cavalcante, V. M. Longo, J. C. Sczancoski, M. A. P. Almeida, A. A. Batista, J. A. Varela and M. O. Orlandi, *CrystEngComm*, 2012, **14**, 853-868.